J Biol Inorg Chem (2007) 12:62–78
DOI 10.1007/s00775-006-0162-1

ORIGINAL PAPER

Characterization of a HoxEFUYH type of [NiFe] hydrogenase from *Allochromatium vinosum* and some EPR and IR properties of the hydrogenase module

Minnan Long · Jingjing Liu · Zhifeng Chen · Boris Bleijlevens · Winfried Roseboom · Simon P. J. Albracht

Received: 23 June 2006 / Accepted: 11 August 2006 / Published online: 13 September 2006

Abstract A soluble hydrogenase from *Allochromatium vinosum* was purified. It consisted of a large (M_r = 52 kDa) and a small (M_r = 23 kDa) subunit. The genes encoding for both subunits were identified. They belong to an open reading frame where they are preceded by three more genes. A DNA fragment containing all five genes was cloned and sequenced. The deduced amino acid sequences of the products characterized the complex as a member of the HoxEFUYH type of [NiFe] hydrogenases. Detailed sequence analyses revealed binding sites for eight Fe–S clusters, three [2Fe–2S] clusters and five [4Fe–4S] clusters, six of which are also present in homologous subunits of [FeFe] hydrogenases and NADH:ubiquione oxidoreductases (complex I). This makes the HoxEFUYH type of hydrogenases the one that is evolutionary closest to complex I. The relative positions of six of the potential Fe–S clusters are predicted on the basis of the X-ray structures of the *Clostridium pasteurianum* [FeFe] hydrogenase I and the hydrophilic domain of complex I from *Thermus thermophilus*. Although the HoxF subunit contains binding sites for flavin mononucleotide and NAD(H), cell-free extracts of *A. vinosum* did not catalyse a H_2-dependent reduction of NAD^+. Only the hydrogenase module (HoxYH) could be purified. Its electron paramagnetic resonance (EPR) and IR spectral properties showed the presence of a Ni–Fe active site and a [4Fe–4S] cluster. Its activity was sensitive to carbon monoxide. No EPR signals from a light-sensitive Ni_a–C* state could be observed. This study presents the first IR spectroscopic data on the HoxYH module of a HoxEFUYH type of [NiFe] hydrogenase.

Keywords Soluble [NiFe] hydrogenase · *Allochromatium vinosum* · Purification · Sequence · NADH:ubiquinone oxidoreductase

Abbreviations

BV	Benzyl viologen
DCIP	2,6-Dichlorophenol-indophenol
EPR	Electron paramagnetic resonance
FMN	Flavin mononucleotide
FPLC	Fast protein liquid chromatography
KPi	Potassium phosphate (50 mM)
MBH	Membrane-bound hydrogenase
MV	Methyl viologen
PAGE	Polyacrylamide gel electrophoresis
SDS	Sodium dodecyl sulfate
SH	Soluble hydrogenase
Tris	Tris(hydroxymethyl)aminomethane–HCl buffer (50 mM)

Introduction

Hydrogenases are found both in prokaryotes and in eukaryotes, where they catalyse the interconversion between H_2 and protons $\left(H_2 \leftrightarrow 2H^+ + 2e^-\right)$. There are three classes: [FeFe] hydrogenases (formerly called

M. Long (✉) · J. Liu · Z. Chen
School of Life Sciences, Bio-energy Center,
Xiamen University, Xiamen 361005,
People's Republic of China
e-mail: longmn@xmu.edu.cn

B. Bleijlevens · W. Roseboom · S. P. J. Albracht (✉)
Swammerdam Institute for Life Sciences,
University of Amsterdam, Nieuwe Achtergracht 166,
1018 WV Amsterdam, The Netherlands
e-mail: asiem@science.uva.nl

[Fe] or Fe-only hydrogenases) [1] with two Fe atoms in the active site [2, 3] coordinated by cyanide and carbon monoxide ligands [4–7], [NiFe] hydrogenases [8], which contain a Ni and an Fe atom in the active site [9, 10], whereby the Fe atom is coordinated by one CO and two CN^- groups [11–14], and [Fe] hydrogenases that have a single Fe atom with two CO ligands [15, 16]. Thus, all hydrogenases have at least one CO as a ligand to Fe in the active site, whereas most have one or more cyanide and cysteine thiol ligands as well. The [FeFe] and [NiFe] hydrogenases also contain Fe–S clusters, which provide a relay for electron transfer to and from the active site which is buried deep inside the protein.

[NiFe] hydrogenases consist of at least two subunits of different size [8, 17, 18]. The larger subunit accommodates the active Ni–Fe site. The smaller subunit contains at least one [4Fe–4S] cluster close to the active site (proximal cluster). In standard [NiFe] hydrogenases, like the *Desulfovibrio gigas* enzyme, this subunit harbours two more clusters: a second cubane cluster (distal cluster) and a [3Fe–4S] cluster (medial cluster) situated between the two cubanes [9, 10].

The active site in standard [NiFe] hydrogenases is a $(CysS)_2Ni(\mu\text{-}'O')(\mu\text{-}CysS)_2Fe(CN)_2(CO)$ centre [9–14, 19–22]. Nickel is coordinated by four thiol groups from cysteine residues, two of which bridge towards Fe. Aerobically purified enzymes are inactive and contain a bridging 'O' species that blocks the active site. There are two different forms of inactive enzyme with different electron paramagnetic resonance (EPR) signals of Ni^{3+}. One form activates within seconds to minutes upon exposure to H_2 and is called the ready state. The other form cannot react with H_2 unless it is first reduced by other means and is called the unready state [23–27]. The 'O' species in both forms was expected to be different [28]. Recent X-ray crystallographic analyses suggest that it is a hydroxide group in the ready enzyme and a peroxide group in the unready enzyme [29, 30].

Many microorganisms can express more than one hydrogenase, as was first described for *Escherichia coli* [31]. It is now known that *E. coli* contains genes encoding for four different [NiFe] hydrogenases [32–34]. The photosynthetic purple sulfur bacterium *Allochromatium vinosum* contains at least two hydrogenases, a membrane-bound hydrogenase (MBH) and a soluble hydrogenase (SH). Evidence for the possible existence of two hydrogenase activities goes back to the 1960s [35–39]. The properties of the solubilized MBH have been thoroughly studied in the Amsterdam group using a variety of techniques, like EPR [8], IR [11–14], stopped-flow IR [25, 40], Mössbauer [41] and X-ray absorption spectroscopy [42, 43]. The purified MBH shows all the physicochemical characteristics of a standard [NiFe] hydrogenase. Also the amino acid sequences of the two subunits [Y. Liang, M. Long, X. Wu, H. Xu and S.P.J. Albracht, unpublished data; UniProtKB/TrEMBL, primary accession numbers Q4KVK0 (large subunit) and Q5XQ37 (small subunit)] are highly similar to those of standard [NiFe] hydrogenases. The DNA-based N-terminus of the small subunit (Q5XQ37) is preceded by EQARR, as determined from protein sequencing (E.C. Bouwens and S.P.J. Albracht, unpublished data).

In this paper, we report on the isolation, purification and characterization of the SH from *A. vinosum*. The purified enzyme consisted of two subunits. The genes encoding for these subunits were cloned and sequenced. They belong to an open reading frame including three more genes. The five genes encode proteins characterizing the enzyme as belonging to the HoxEFUYH type of [NiFe] hydrogenases first found in *Cyanobacteria* [44–48] and more recently also in *Thiocapsa roseopersicina* [49]. The purified enzyme represented only the hydrogenase module (HoxYH). Detailed sequence comparisons showed that the intact HoxEFUYH complex may contain three [2Fe–2S] clusters and five [4Fe–4S] clusters. We predict that its basic structure is like that of the domains formed by the subunits Nqo2 (24 kDa), Nqo1 (51 kDa) and the N-terminal part of Nqo3 (75 kDa) from the hydrophilic fragment of *Thermus thermophilus* NADH:ubiquinone oxidoreductase (complex I), the X-ray structure of which has been published recently [50–52].

Materials and methods

Cell growth and harvest

A. vinosum strain DSM 185 was grown in a 700-l batch culture [53] in a medium as described before [54, 55]. The cells were harvested by means of a Sharples MP4 continuous-flow centrifuge and stored at –20 °C.

Small-scale purification of the SH

Frozen cells (50-g wet weight) were thawed in a cold room (4 °C) overnight. The cell paste was suspended in 200 ml cold 50 mM tris(hydroxymethyl)aminomethane–HCl buffer (Tris) of pH 8.0 and stirred for 20 min at 4 °C. The suspension (cooled in an ice–water bath) was then treated with ultrasound (10 × 2 min with intermittent cooling) with a Branson Sonifier (W-380, Heat Systems, Farmington, NY, USA) at an output

setting of 8 and centrifuged at 20,000*g* for 30 min to remove unbroken cells and cell walls. The supernatant was centrifuged at 200,000*g* for 90 min. The clear supernatant was applied onto a (diethylamino)ethyl (DEAE)–cellulose column (Whatman DE-52; 60 cm × 5 cm) equilibrated with Tris (pH 7.4). The column was washed with two bed volumes of starting buffer. Subsequently, a linear salt gradient (0–0.4 M NaCl in Tris pH 7.4) was applied. Two H_2-production activity peaks were observed. The first one occurred around 0.25 M NaCl and contained the SH. Active fractions were pooled and dialysed against 10 mM Tris–HCl buffer (pH 8.0). The second peak, which occurred around 0.3 M NaCl, contained some MBH and was discarded. The dialysed SH solution was applied onto a TSK–DEAE 650 (M) column (Merck; 28 cm × 3 cm). The contents of the column were eluted batchwise with two bed volumes each of 0.1, 0.13 and 0.15 M NaCl in Tris (pH 8.0). The active fractions were combined, concentrated to about 0.5 ml and then applied onto an Ultragel ACA-44 column (LKB; 180 cm × 1.5 cm), which was equilibrated with 0.1 M NaCl in Tris (pH 8.0); the flow rate was adjusted to about 45 ml h^{-1}. The active fractions were pooled, dialysed against 20 mM Tris–HCl buffer (pH 8.0) and applied onto a fast protein liquid chromatography (FPLC) Mono-Q column (Pharmacia). The contents of the column were eluted with a linear salt gradient (0–0.3 M NaCl) in Tris (pH 8.0).

Large-scale purification of the SH and purification of the MBH

A bacterial cell paste (500 g) was subjected to an acetone-extraction procedure [56] to remove lipids and photosynthetic pigments. The resulting dry powder (190 g) was suspended in 600 ml Tris (pH 7.4) and stirred for 30 min at 4 °C. The suspension was centrifuged at low speed (1,000*g*) for 10 min and the pellet was extracted once more with 400-ml buffer. The combined extracts were subjected to a high-speed centrifugation step (35,000*g*, 45 min) and applied onto a DEAE–cellulose column (Whatman DE-23; 65 cm × 7 cm). The column was first washed with 5 l Tris (pH 7.4). Hydrogenases were eluted with a linear NaCl gradient (0–0.5 M). The second activity peak was used for the purification of the MBH as described earlier [57]. The purification of the SH (first activity peak) was performed by using a TSK-DEAE column and an AcA-44 column. Then a second TSK-DEAE column step with a linear gradient elution (0–0.25 M NaCl) was applied. Thereafter the hydrogenase was further purified by a FPLC Superdex 200 column (Hiload 16/60), the contents of which were eluted with Tris (pH 8.0), containing 0.1 M NaCl, at a rate of 0.5 ml min^{-1}. All purification steps were performed between 4 and 8 °C, except for those involving the FPLC columns, which were run at room temperature. Preparations were stored in liquid nitrogen until further use. Protein was determined according to the method of Lowry et al. [58] with bovine serum albumin as a standard.

Activity measurements

Hydrogenase activities were measured at 30 °C in a 2.1-ml cell with a Clark electrode (type YSI 5331) for polarographic measurement of H_2 [59]. Hydrogen-production activity was determined in 50 mM potassium phosphate (KPi) buffer (pH 6.0), 1.5 mM methyl viologen (MV), 50 mM dithionite and an appropriate amount of enzyme. The H_2-uptake activity of the SH was measured in KPi buffer (pH 7.4). For the MBH, Tris (pH 8.0), containing 2.2 M KCl, was used. A final concentration of 40 μM H_2, 2.0 mM benzyl viologen (BV) and an appropriate amount of enzyme was added. Just before the start of the reaction, 50 μM dithionite was added to remove oxygen and to activate the enzyme.

Native gel electrophoresis, activity staining and subunit composition

Native gel electrophoresis was conducted in a flat-gel apparatus for vertical slabs [60] using the buffer system of Laemmli [61]. The polyacrylamide concentration was 3.5% for the stacking gel and 7.5% for the running gel. A current of 20 mA was used for the stacking gel and 30 mA for the running gel. Duplicate samples were applied. After the run, the gel was divided into two parts. One part was stained for protein by incubation in a staining solution (0.25% Coomassie brilliant blue R-250, 10% acetic acid and 40% methanol) for 30 min and subsequent destaining in 10% acetic acid and 40% methanol. The other part was stained for activity by incubating the gel in a reaction buffer (KPi buffer pH 6.0, 50 mM 2-mercaptoethanol and 1 mM MV) for 30 min at room temperature. After discarding the liquid phase, the gel was kept under 100% H_2 at room temperature. When the blue colour of reduced MV appeared, an anaerobic solution of 2.5% 2,3,5-triphenyl-2*H*-tetrazoliumchloride was added and the gel was kept under 100% Ar for 20 min [31, 62, 63].

To determine the subunit composition, the activity band was cut out from the native gel and incubated at room temperature in a denaturing buffer (1.25 M Tris–HCl, pH 6.8, 13% glycerol, 5% sodium dodecyl sulfate (SDS), 0.003% bromophenol blue and 0.14 M 2-mercaptoethanol) for 20 min at room temperature. Thereafter the enzyme was further denatured at 100 °C for 5 min and subjected to SDS polyacrylamide gel electrophoresis (PAGE) with 0.5% SDS [61]. The apparent molecular mass of the subunits was determined by the R_f value relative to standard protein markers (94, 67, 30, 20.1 and 14.4 kDa; Pharmacia).

Analysis of N-terminal sequences of the SH and DNA sequencing

After activity staining, the activity band was cut out from the native gel and denatured in SDS buffer as described already. After SDS-PAGE, the bands of the subunits were electroblotted onto a poly(vinyl formal) membrane [64] with an electroblot instrument (semi-dry transfer, Bio-Rad), cut out and used for N-terminal amino acid analysis by automated Edman degradation using an Applied Biosystems 470A gas-phase protein sequencer.

On the bais of the N-terminal amino acid sequences of the large and small subunits of the SH, two sets of PCR primers were synthesized. The genomic DNA from *A. vinosum* was extracted [65] and the gene encoding the small subunit was cloned by standard PCR procedures [65]. DNA sequencing was performed using dye-primer chemistry (Base-Clear, Leiden, The Netherlands). To obtain the complete sequence of the SH, the genomic DNA was first digested with restriction endonuclease *Bam*HI. It was then ligated with an adapter containing *Bam*HI cohesive ends. PCR primers were designed according to the upstream sequence of the small subunit and the sequence of the adapter. The sequences of the large subunit and the accessory genes were cloned by PCR using the ligation product as a template. DNA sequencing of double strands was performed by the Shenggong Company (Shanghai, China). Sequences have been submitted to the NCBI/GenBank databases (AY944574).

IR and EPR spectrometry

IR and EPR spectra were obtained as before [14, 66]. For IR measurements, the enzyme samples were concentrated in a Millipore Centricon YM-10 centrifugal filter unit.

Results

Small-scale purifications

When *A. vinosum* cells were treated with ultrasound, two types of hydrogenase activities could be detected in the supernatant after the high-speed centrifugation step (90 min at 200,000*g*) by using the H_2-uptake assay in native gels. As observed before [57], the enzymes responsible for the two activities could be separated at the first column (DE-52). One activity peak appeared to be due to the SH and appeared at 0.25 M salt. The second activity peak, due to some solubilized MBH, occurred at a higher salt concentration (0.3 M). The majority of the MBH activity was found in the pellet after the high-speed centrifugation step.

Identification of the two hydrogenases was performed by native PAGE analysis (Fig. 1, lanes A–F).

Activity staining showed that the two activity peaks clearly differed in mobility. The second activity peak exhibited the same electrophoretic properties as the purified MBH.

As shown later, the SH showed a greater activity in the H_2-production assay than in the H_2-uptake reaction when compared with the MBH; therefore, the two peaks in the activity profile of the DE-52 column were best recognized when the fractions were assayed for H_2 production. On the second column (TSK-DEAE), the SH was eluted at 0.13 M NaCl, and 67% of the activity

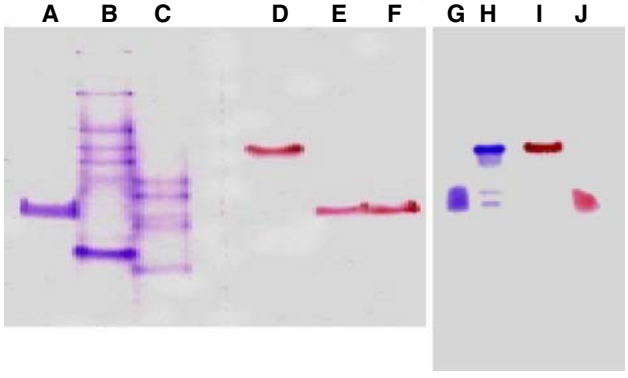

Fig. 1 Native polyacrylamide gel electrophoresis (*PAGE*) analysis of fractions during the small-scale purification procedure. *Lanes A–F* show the analysis of the two activity peaks from the DE-52 column. *A*, *F* Control with purified membrane-bound hydrogenase *(MBH)* from *Allochromatium vinosum*. *B*, *D* A sample from the first activity peak. *C*, *E* A sample from the second activity peak. *Lanes G–J* show the analysis of the purified soluble hydrogenase (*SH*). *G*, *J* Control with purified MBH from *A. vinosum*. *H*, *I* Purified SH. *Lanes A–C*, *G* and *H* were stained with Coomassie brilliant blue and *lanes D–F*, *I* and *J* were stained for activity. Protein bands run from *top* (negative) to *bottom* (positive)

Table 1 Small-scale purification of the soluble hydrogenase activity from *Allochromatium vinosum*, starting with 50 g (wet weight) of cells

Step	Total protein (mg)	Total activity (U)	SA (U mg^{-1})	Purification (fold)	Yield (%)
DE-52	230	22.0	0.096	1	100
TSK-DEAE	20.8	14.7	0.71	7.4	67
AcA-44	4.2	11.4	2.71	28.2	52
FPLC Mono-Q	1.1	8.3	7.5	78.1	37

SA specific H_2-production activity, *DEAE* diethylaminoethyl, *FPLC* fast protein liquid chromatography

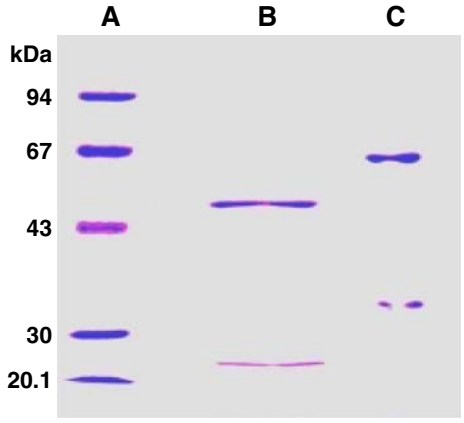

Fig. 2 Sodium dodecyl sulfate PAGE analysis of the SH from *A. vinosum*. *A* Standard protein markers (94, 67, 43, 30 and 20.1 kDa). *B* SH. *C* Purified MBH from *A. vinosum*. The concentration of the gel was 7.5%

was recovered and a sevenfold purification was achieved. The third column (AcA-44) yielded another fourfold purification, and 78% of enzyme activity was recovered. As a last purification step, an FPLC Mono-Q column was used. The activity was eluted at 0.17 M NaCl. Native-gel analyses indicated that the SH was still not absolutely pure (Fig. 1, lane H).

After four purification steps, the SH from *A. vinosum* was purified 78-fold with a yield of 37% and a specific H_2-production activity of 7.5 U mg^{-1} of protein (in KPi buffer at pH 6.0). The purification procedure is summarized in Table 1.

Determination of the subunit composition of the SH

The purified SH was subjected to a native PAGE treatment. After identification of the SH band by activity staining, the band was sliced out and used for SDS-PAGE. Two bands were observed after Coomassie brilliant blue staining (Fig. 2).

The apparent molecular mass of the two subunits was determined as 52 and 23 kDa. This fits nicely with the masses predicted from the amino acid sequences (HoxH, 53.5 kDa; HoxY, 19.8 kDa) as reported later.

Amino acid sequences

For the small hydrogenase subunit, the N-terminal sequence deduced from the DNA was STQPKITVATAWLDG; this was identical to the N-terminal sequence of the protein (STQPKITVATxxLDG). The absence of a leader sequence points to a cytoplasmic location of this soluble enzyme. For the large subunit, the DNA-based N-terminal sequence was SRTITIEPVTRIEGHAR and matched the protein N-terminal sequence (SRTITIEPVTRxEGHAR). The genes encoding for the small and large hydrogenase subunits were preceded by three other genes which appeared to be highly similar to the *hoxEFU* genes found in a number of other organisms [44–47, 49].

Inspection of the HoxEFUYH subunits for binding motifs of prosthetic groups and substrates

A decade ago Schmitz et al. [44] reported a detailed sequence analysis of the HoxEFUYH subunits of the hydrogenase from *Cyanobacteria*. They corroborated and extended the several evolutionary links reported earlier for this type of enzyme to subunits of NADH:ubiquinone oxidoreductase (complex I) and the *Clostridium pasteurianum* [FeFe] hydrogenase I. In the meantime, the X-ray structures of the two latter enzymes have appeared and many new sequences have been added to the databases. This prompted us to reexamine the similarities of the five subunits of the *A. vinosum* HoxEFUYH complex with known sequences. To this purpose, BLAST searches [67] with the five subunits were performed at ExPASy in the UniProtKB database and the 60 most similar sequences were aligned with CLUSTAL X (1.64b) [68]. The main results are given in the following subsections.

The HoxE subunit

The HoxE subunit of *A. vinosum* has a cysteine motif **C**x_4**C**x_{35}**C**x**G**x**C**x_3P (x denotes a nonconserved residue; residues predicted to bind an Fe–S cluster are printed in bold and have the same notation) in common with all of the 60 most similar sequences. The 24-kDa subunit of complex I, which is amongst them, contains a [2Fe–2S] cluster as originally demonstrated for the bovine enzyme by Ohnishi et al. [69–71].

The recently published structure of the *T. thermophilus* 24-kDa (Nqo2) subunit demonstrates that this [2Fe–2S] cluster is indeed bound by the **C**x$_4$**C**x$_{35}$**C**x**G**x**C**x$_3$P motif [51]. We predict that the *A. vinosum* HoxE also contains a [2Fe–2S] cluster (Table 2).

The HoxF subunit

The *A. vinosum* HoxF subunit and many of the other 60 sequences contain a cysteine motif in the N-terminal region (**C**x$_4$**C**x$_{28–30}$G**C**x$_3$**C**x$_3$PL), which could host an additional Fe–S cluster. As noted before [44], this motif is highly similar to the cysteine motif in the HoxE-like proteins (**C**x$_4$**C**x$_{35}$**C**x$_3$**C**x$_3$P) discussed earlier and this suggests that also the HoxF subunits may contain a [2Fe–2S] cluster (Table 2).

Further on in the HoxF sequence, several motifs homologous to those in the 51-kDa subunit of complex I are present. The X-ray structure of the 51-kDa (Nqo1) subunit in the *T. thermophilus* complex I [51] shows that these motifs, within residues 73–240, are involved in the binding of a flavin mononucleotide (FMN) group and also have the capacity to bind NAD(H). The HoxF-like sequences are highly similar to this stretch of residues starting with the RGRGG motif up to the motif INNVET at the end of this stretch (Table 2); hence, it can safely be concluded that the binding sites for FMN and NAD(H) are also present in HoxF. The presence of a glutamic acid residue in the conserved CGEETAL motif within this stretch of residues suggests that the subunits bind NAD(H) rather than NADP(H) because the glutamic acid residue forms a hydrogen bond with the 2′-OH of the adenine ribose ring of NAD(H). This glutamic acid residue would repel the phosphate group in this position in NADP(H) [72, 73].

A conserved cysteine motif **C**G**C**x$_2$**C**RxG-x$_{35}$–L**C**x$_2$G on the C-terminal side of the FMN/NAD(H) binding motifs is present in all of the 60 similar sequences, including the 51-kDa subunit of complex I. The structure of the *T. thermophilus* 51-kDa (Nqo1) subunit shows that a [4Fe–4S] cluster is bound to a **C**x$_2$**C**x$_2$**C**x$_{40}$**C** motif; hence we predict that the *A. vinosum* HoxF binds a [4Fe–4S] cluster, even though the spacing between the third and the fourth cysteine residue is one residue shorter than the spacing found in the 51-kDa subunit.

Table 2 Important sequence motifs in the subunits of the HoxEFUYH [NiFe] hydrogenase of *A. vinosum* and homologous sequences

Subunit	Motif[a]	Predicted binding site for	Homologous sequences containing this motif
HoxE	Cx$_2$**C**x$_4$**C**-x$_{35}$–**C**x**G**x**C**x$_3$P	**[2Fe–2S]** cluster	24 kDa of complex I
HoxF	**C**x$_4$**C**x$_{28–30}$G**C**x$_3$**C**x$_3$PL	**[2Fe–2S]** cluster	24 kDa of complex I; not present in 51 kDa of complex I or HoxF of *Ralstonia eutropha*
	RGRGGxGYP-x$_{145–154}$–INNVET	Flavin mononucleotide and NAD(H)	51 kDa of complex I and HoxF of *R. eutropha*
	FCx$_2$ES**C**GK**C**xP**C**Rx$_{26}$ExLCx$_7$L**C**G**L**G	**[4Fe–4S]** cluster	51 kDa of complex I and HoxF of *R. eutropha*
HoxU	**C**x$_{10}$**C**x$_2$**C**x$_{13}$**C**-x$_{33}$–	**[2Fe–2S]** cluster	*Clostridium pasterianum* [FeFe] hydrogenase I, 75 kDa of complex I and HoxU of *R. eutropha*
	Hx***C***x$_2$***C***x$_5$***C***-x$_{38}$–	***[4Fe–4S]*** cluster with histidine ligand	*C. pasterianum* [FeFe] hydrogenase I, 75 kDa of complex I (both with ***H***x$_3$***C***); *not* in *R. eutropha* HoxU
	Cx$_2$**C**x$_2$**C**x$_3$***C***-x$_{33}$–***C***x$_2$**C**x$_2$***C***x$_3$**C**P	[**4Fe–4S**] and ***[4Fe–4S]*** cluster	[FeFe] hydrogenases (**distal** and ***medial*** to the Fe-Fe active site); ***medial*** cluster *not* in 75 kDa of complex I or HoxU of *R. eutropha*
HoxY	**C**x$_2$**C**-x$_n$–Gx**C**A-x$_m$–G**C**PP	**[4Fe–4S]** cluster proximal to Ni–Fe active site	All [NiFe] hydrogenases, all PSST subunits (20 kDa) of complex I (which have CC instead of Cx$_2$C)
HoxH	**C**Gx**C**	N-terminal cysteine ligands to Ni–Fe active site	All [NiFe] hydrogenases
	GxxEAPRGxL	Arginine residue capping the Ni–Fe active site	All [NiFe] hydrogenases
	DP**C**x$_2$**C**x$_2$H	C-terminal cysteine ligands to Ni–Fe active site	All [NiFe] hydrogenases

[a] Order of motifs is from N- to C-terminus. Only the residues in *bold* are involved in the predicted binding of the Fe–S clusters or of the Ni–Fe centre

The HoxU subunit

Almost all of the 60 sequences most similar to the HoxU subunit from the soluble *A. vinosum* enzyme have four cysteine motifs in common that have nearly the same spacing: **C**x_{10}**C**x_2**C**x_{13}**C**-$x_{31,33}$–**H**$x_{1,3}$**C**x_2**C**x_5**C**-$x_{38–53}$–**C**x_2**C**x_2**C**x_3**C**-$x_{31–33}$–**C**x_2**C**x_2**C**x_3**C**P ($x_{31,33}$ means 31 or 33 residues; $x_{31–33}$ means 31 to 33 residues). Pilkington et al. [72] discovered that the *Ralstonia eutropha* HoxU protein has a sequence similar to the first 240 amino acids of the 75-kDa subunit of bovine complex I. Later it was recognized that this stretch was also similar to the first 201 amino acids of the sequence from the [FeFe] hydrogenase I of *C. pasteurianum* [8, 74]. In fact, the *C. pasteurianum* hydrogenase contains a **C**x_{11}**C**x_2**C**x_{12}**C**-x_{31}–***H***x_3***C***x_2***C***x_5***C***-x_{39}–**C**x_2**C**x_2**C**x_3***C***-x_{32}–***C***x_2***C***x_2***C***x_3**C**P motif (residues predicted to bind a particular Fe–S cluster [74] are printed in bold and have the same notation) which is nearly identical to that found in the HoxU subunit. The 75-kDa subunit of bovine complex I has a similar motif but lacks the four *cysteine* residues (motif is **C**x_{10}**C**x_2**C**x_{13}**C**-x_{31}–***H***x_3***C***x_2***C***x_5***C***-x_{38}–**C**x_2**C**x_2**C**-x_{43}–**C**P). Because the rest of the sequences of these two proteins differ greatly from that of HoxU, they did not score well in the BLAST search with HoxU. Yet, they are of great interest because the 3D structure of both proteins is now known.

In 1998, the crystal structure of the *C. pasteurianum* hydrogenase I was published [2] and shortly afterwards that of the *D. desulfuricans* enzyme appeared [3]. Both hydrogenases contain the H cluster (hydrogen-activating cluster), which consists of a $[2Fe]_H$ subcluster, with CO and CN^- ligands [5, 7], linked via a cysteine thiol to a [4Fe–4S] cluster called the $[4Fe–4S]_H$ subcluster. In addition there are two [4Fe–4S] clusters, one close to the H cluster (medial cluster) and one further away (distal cluster). The *C. pasteurianum* enzyme has an N-terminal extension binding a fourth [4Fe–4S] cluster and a [2Fe–2S] cluster. In this enzyme the H cluster is bound by the C-terminal part of the protein, whereas the four Fe–S clusters are bound by the first 201 N-terminal amino acids. On the basis of the crystal structures of the [FeFe] hydrogenases, we predict the following for the *A. vinosum* HoxU subunit (Table 2). The first four cysteine residues in the N-terminal region may bind a **[2Fe–2S]** cluster. The second motif, with three cysteine ligands and one histidine ligand, possibly binds a ***[4Fe–4S]*** cluster. The spacing between the conserved histidine residue and the following cysteine residue is HxC in the *A. vinosum* HoxU, but HxxxC in the [FeFe] hydrogenase. Yet, the spacing between the last cysteine residue in the **[2Fe–2S]**-binding motif and the first cysteine residue in the ***[4Fe–4S]***-binding motif is the same, 35 residues. The two remaining cysteine motifs probably bind two [4Fe–4S] clusters, which in the [FeFe] hydrogenases are the **distal** and ***medial*** clusters, respectively. We note that, just like the 75-kDa subunits of complex I, the HoxU subunit of *R. eutropha* lacks the four conserved cysteine residues that bind the ***medial [4Fe–4S]*** cluster in [FeFe] hydrogenases.

Interestingly, the calculated isoelectric point of the *A. vinosum* HoxU subunit is 7.5. This value is much closer to that of the homologous N-terminal sequence of the 75-kDa subunit of bovine complex I (8.2) than to those of the homologous N-termini of the [FeFe] hydrogenase I (5.4) or the *T. thermophilus* 75-kDa (Nqo3) subunit (5.5). In general, Fe–S proteins are rather acidic.

The HoxY subunit

The *A. vinosum* HoxY subunit has homologues in a group of [NiFe] hydrogenases that carry only one Fe–S cluster in the hydrogenase module, because there is only one conserved cysteine motif: **C**xG**C**-x_n–Gx**C**A-x_m–G**C**PP. This typical pattern binds the proximal [4Fe–4S] cluster, close to the Ni–Fe site, in all [NiFe] hydrogenases [8, 17].

Also quite a number of sequences annotated as 'NADH ubiquinone oxidoreductase, 20-kDa subunit' showed up in the BLAST search. In bovine complex I, this subunit [75] is often called the PSST subunit after its first four amino acids [76]. As described earlier, both the small subunits of hydrogenases and the PSST subunits of NADH:Q oxidoreductases have stretches of amino acids in common which in [NiFe] hydrogenases form a conserved flavodoxin fold [77]. In the NAD^+-reducing [NiFe] hydrogenase from *R. eutropha*, this flavodoxin fold is proposed to bind one of the two FMN groups in this enzyme [77, 78], namely the FMN responsible for the radical EPR signal in the reduced enzyme [79].

Also in bovine complex I the predicted flavodoxin fold in the PSST subunit is expected to bind the second FMN present in the intact complex [77, 80]. It was gratifying to see that the PSST (Nqo6) subunit of *T. thermophilus* indeed contains the predicted flavodoxin fold, although no bound FMN was detected [51, 52]. This FMN may be lost during the purification of the hydrophilic domain, where the stabilizing effects of the membrane-bound domain and the phospholipids are removed. Also in the soluble NAD^+-reducing [NiFe] hydrogenase from *R. eutropha* this FMN is readily lost [78]. For the *T. thermophilus* complex I it

has not yet been shown whether the specific reaction site for NADPH, which is present in bovine complex I [81] and the HoxFUYHI$_2$ [NiFe] hydrogenase from *A. eutrophus* [79, 82], is functional.

The HoxH subunit

As expected, the *A. vinosum* HoxH subunit is similar to virtually all large subunits of [NiFe] hydrogenases in that it has the two well-known cysteine motifs that bind the active site: a **C**Gx**C** motif in the N-terminal region and a DP**C**xx**C**xxH at the C-terminus. At some distance before the second cysteine motif a GxxEAPRGxL motif contains the strictly conserved arginine residue which acts as a cap on the Ni–Fe active site as observed in all crystal structures of these enzymes [9, 10, 21, 22, 29, 30, 83–87]. As predicted by earlier sequence comparison [77],the structure around the Ni–Fe site is indeed preserved in the X-ray structure of the homologous 49-kDa (Nqo4) subunit in complex I from *T. thermophilus* [51].

In summary, inspection of the sequences of the subunits of the *A. vinosum* HoxEFUYH complex predicts the presence of eight Fe–S clusters (Table 2).

Large-scale purification

As described already, the purification starting with 50 g of cells yielded only about 1 mg of purified HoxYH enzyme. In order to study some enzymological and spectral properties of the enzyme, a large-scale purification procedure was developed starting with 500 g of cells. In this case the sonification method was inadequate to open up the cells. We therefore tried to use the dry powder obtained after acetone extraction of the cells [56] as the starting material, a method successfully applied for the isolation and purification of the MBH [57]. As a result, also a large amount of the MBH was present after buffer extraction of the dry powder. With a DE-23 column as the first column, the HoxYH enzyme could be separated nearly completely from the MBH. Nevertheless, an extra TSK–DEAE column was invoked in the subsequent purification to eliminate trace amounts of the MBH. The large-scale purification procedure is summarized in Table 3.

After five purification steps, the HoxYH enzyme from *A. vinosum* was purified 52-fold with a yield of 39% and a specific H_2-production activity of 8.4 U mg^{-1} of protein (in KPi buffer, pH 6.0). Apparently the acetone treatment of the cells had no effect on the properties of the HoxYH enzyme when compared with the small-scale procedure where cells were disrupted by ultrasound. The procedure was performed three times and was quite reproducible. The amount of purified enzyme was 10–15 mg from 500 g of cells. We noted that a concentrated enzyme solution (40–60 mg ml^{-1}) as required for EPR had a pinkish-brown colour.

Table 3 Large-scale purification of the soluble hydrogenase activity from *A. vinosum*, starting with 500 g (wet weight) of cells

Step	Total protein (mg)	Total activity (U)	SA (U mg^{-1})	Purification (fold)	Yield (%)
DE-23	1,744	282	0.162	1.0	100
TSK-DEAE (I)	494	241	0.48	3.0	85
AcA-44	148	180	1.22	7.5	64
TSK-DEAE (II)	61	146	2.40	14.8	52
FPLC Superdex	13	109	8.4	51.9	39

SA specific H_2-production activity

Enzymological, EPR and IR properties of the HoxYH enzyme

As described already, the purified enzyme consisted only of the HoxYH subunits. This means that the HoxEFUYH complex apparently breaks up or dissociates upon destruction of the cells. This may explain why we, in accordance with earlier observations [36, 38], could not find any $H_2 \rightarrow NAD^+$ activity in cell-free extracts.

The calculated p*I* values for the *A. vinosum* HoxYH and MBH [NiFe] hydrogenases were 5.9 and 5.4, respectively. This slight difference is in agreement with the difference in mobility of the two enzymes on native gels, i.e. the more positive HoxYH enzyme runs more slowly to the positive pole than the solubilized MBH.

The optimum pH for the H_2-production activity of the HoxYH enzyme in KPi buffer was about 6.0 (not shown). Whereas the MBH of *A. vinosum* is quite stable at higher temperatures (e.g. little loss of activity after 10 min at 65 °C [53, 88]), the HoxYH enzyme was not. At temperatures up to 40 °C, the enzyme was stable for up to 1 h in air (not shown). When kept for 1 h at 50 °C, about 30% of the activity was lost. At 60 °C, the loss was about 70%, whereas at 70 °C, no activity could be measured anymore after 1 h. No significant loss of activity was noticed after storage for several weeks at –20 °C.

The *A. vinosum* MBH is very resistant to trypsin and chymotrypsin degradation, e.g. when incubated with chymotrypsin at 37 °C for 1 h, almost no activity is lost. In fact, a treatment with chymotrypsin is routinely used during the MBH purification to eliminate contaminating proteins [57]. The HoxYH enzyme of *A. vinosum*

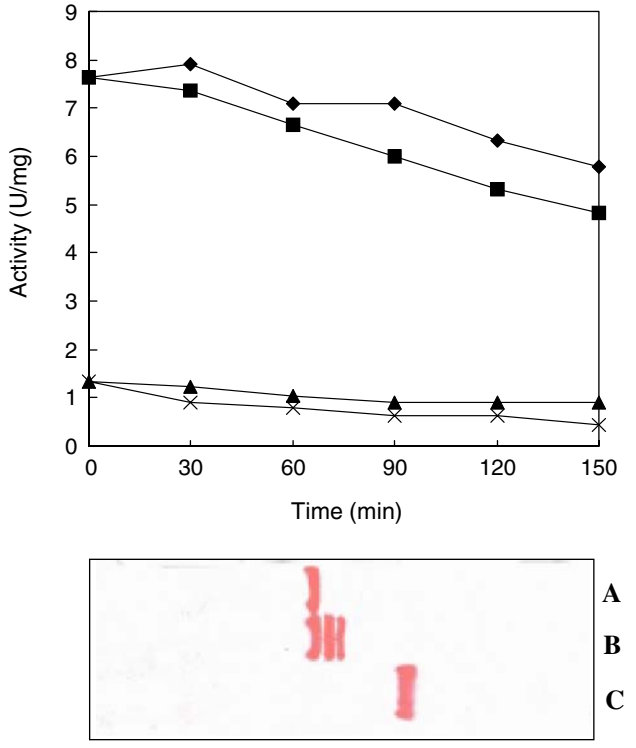

Fig. 3 Effect of trypsin on the *A. vinosum* HoxYH enzyme at 37 °C. The purified HoxYH enzyme, in 50 mM tris(hydroxymethyl)aminomethane–HCl buffer (pH 8.0), was incubated with trypsin (40 U mg^{-1} hydrogenase protein) at 37 °C. *Upper panel*: Every 30 min a sample was taken for activity measurements. *Diamonds* H_2-production activity of a control sample. *Suares* H_2-production activity of the trypsin-treated sample. *Triangles* H_2-uptake activity of the control sample. *Crosses* H_2-uptake activity of the trypsin-treated sample. *Lower panel*: A sample incubated for 90 min was used for activity staining in a native PAGE. *A* Untreated HoxYH enzyme. *B* Trypsin-treated HoxYH enzyme. *C* Untreated MBH. Protein bands run from *left* (negative) to *right* (positive)

was somewhat less stable in the presence of trypsin. A slight but noticeable inactivation was observed when the enzyme was incubated with trypsin at 37 °C. Native PAGE showed that the enzyme was partly digested by trypsin and that two of the degradation products still exhibited hydrogenase activity (Fig. 3).

Several electron carriers were tested for their reactivity with the HoxYH enzyme (not shown). The maximum H_2-production activity (8.1–8.4 U mg^{-1}) was obtained with dithionite-reduced MV. BV was the best electron acceptor in the H_2-uptake assay (2.6 U mg^{-1}). Also horse-heart cytochrome *c* as an electron acceptor gave some activity (0.3 U mg^{-1}) in the latter assay. The HoxYH enzyme showed no activity with NAD(H), NADP(H) or $K_3Fe(CN)_6$. The H_2-uptake reaction with MV (0.75 U mg^{-1}) was 10 times lower than the H_2-production reaction with MV.

Most hydrogenases are inhibited by CO in a way competitive towards dihydrogen. We tested the sensitivity of the HoxYH enzyme to CO in the H_2-production reaction (Fig. 4a). Half-maximal inhibition was obtained with about 3 μM CO. We compared this with the CO sensitivity of the MBH in the H_2-production reaction (Fig. 4b). In this case the activity was already 50% inhibited at a concentration of about 0.25 μM.

The amino acid sequences of the HoxYH subunits strongly indicated that the enzyme from *A. vinosum* is a [NiFe] hydrogenase with one [4Fe–4S] cluster. To obtain further evidence for this, the HoxYH enzyme obtained from the large-scale purifications was inspected by EPR (Fig. 5). Wide-field scans of the untreated enzyme at 45 and 10 K showed several signals (Fig. 5, panel I):

1. A prominent rhombic signal around $g = 4$ ($g_{123} = 4.76$, 4.047, 3.73). It is assigned to the middle doublet of an $S = 5/2$ system with rhombic symmetry. By treating it as an apparent $S = 1/2$ signal, we obtained an estimated spin concentration (by direct double integration) of 107 μM.

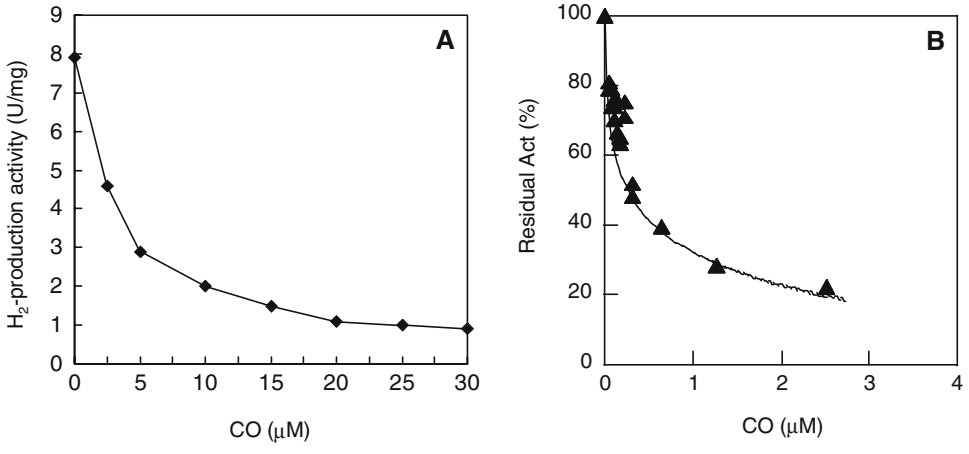

Fig. 4 Comparison of the inhibitory effects of CO on the H_2-production reactions catalysed by the HoxYH enzyme and MBH from *A. vinosum*. Different amounts of CO-saturated buffer were added to the reaction buffer. The H_2-production activity was detected with dithionite-reduced methyl viologen as an electron donor. **a** Inhibition of the HoxYH enzyme. **b** Inhibition of the MBH

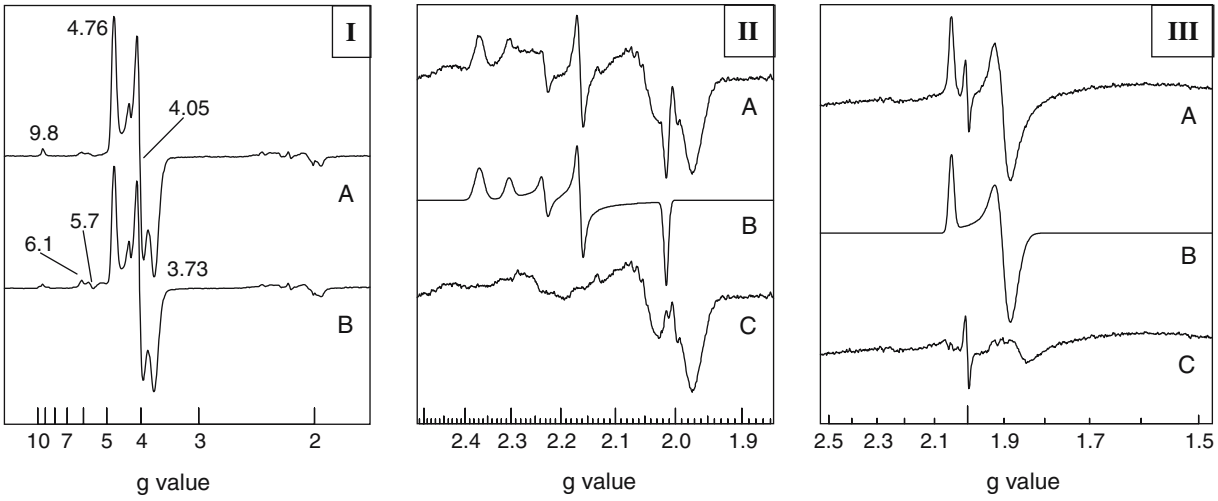

Fig. 5 Electron paramagnetic resonance spectra of the HoxYH enzyme. *Panel I*: Wide-field scans of untreated enzyme. *A* Spectrum at 45 K and a microwave power attenuation of 20 dB (0 dB = 260 mW). *B* Spectrum at 10 K and 30 dB. *Panel II*: Spectra of untreated enzyme in the $g = 2$ region. *A* Spectrum recorded at 45 K and 20 dB. *B* Simulation of the nickel signals as the sum of two $S = 1/2$ spectra. The parameters for the signal of the Ni_r* state are $g_{123} = 2.3685, 2.1638, 2.0165$; widths(123) = 2.45, 1.25, 1.25 mT. The parameters for the signal of the Ni_u* state are $g_{123} = 2.3043, 2.2315, 2.0165$; widths(123) = 2.05, 1.38, 1.15 mT. *C* Difference spectrum *A* minus *B*. *Panel III*: Spectrum of the HoxYH enzyme treated with H_2 as described in the text. *A* Spectrum recorded at 12 K and 30 dB. *B* Simulation as a $S = 1/2$ spectrum. Parameters $g_{123} = 2.0453, 1.8998, 1.8786$; widths(123) = 2.50, 5.50, 8.21 mT. *C* Difference spectrum *A* minus *B*

Taking into consideration that the signal represents only the spins in the middle doublet and assuming an equal population of all three doublets at 45 K, we have to multiply this concentration by 3, so the signal represents a species with a concentration of 322 μM. At 10 K, a direct double integration gave an apparent spin concentration of 74 μM, in agreement with a depopulation of the middle doublet at lower temperatures.

2. Two small lines at $g_1 = 6.1$ and $g_2 = 5.7$, ascribed to an $S = 5/2$ system with nearly axial symmetry, presumably a high-spin haem.
3. A small peak at $g = 9.82$ and one at $g = 9.36$, which had a different temperature dependence. These lines are assigned to the other doublets of the rhombic $S = 5/2$ system.

There was no signal attributable to an oxidized $[3Fe–4S]^+$ cluster. At 45 K two weak signals due to Ni^{3+} were noticed. This is shown in detail in trace A of panel II in Fig. 5. The signals could be simulated as a summation of two $S = 1/2$ signals. The close analogy of the g values with those of the Ni signals of the *A. vinosum* MBH led us to ascribe the signals to the Ni_r* state (with $g_{123} = 2.37, 2.16, 2.02$) and the Ni_u* state (with $g_{123} = 2.30, 2.23, 2.02$). The combined signal intensity amounted only to 4.2 μM. The signal obtained after subtraction of the simulated Ni spectra is reminiscent to that of Cu^{2+} as found in type-II copper proteins or in proteins which have aspecifically bound copper [89].

When the solution was placed under H_2 (evacuation and flushing eight times) for 16 h at 4 °C, no changes were observed. A subsequent incubation under H_2 at room temperature (20 °C) for 4.5 h did change the spectrum. The $g = 4$ signal collapsed to half of its original amplitude, the $g = 6$ signals as well as the Ni^{3+} signals disappeared and a new signal appeared in the $g = 2$ region. It was optimally sharpened at 12 K (Fig. 5, panel III). This property and its g values ($g_{123} = 2.05, 1.90, 1.88$) identify it as due to a reduced [4Fe–4S] cluster. In view of the cysteine motif in the HoxY subunit, we assign the signal to the proximal [4Fe–4S] cluster. The estimated spin concentration of the signal, obtained from the simulation, was 6.2 μM. The signal around $g = 4$ disappeared completely only upon addition of excess dithionite plus MV (not shown).

Two more preparations from large-scale purifications were inspected by EPR. Both showed the strong signal around $g = 4$ as well as the nickel-based signals. The ratio of the Ni_r* and Ni_u* signals varied, as is often observed with [NiFe] hydrogenases. In none of the preparations could the characteristic light-sensitive EPR signal of the Ni_a–C* state be induced using methods which gave an optimal Ni_a–C* signal with the MBH, e.g. flushing with Ar or 1% H_2 after reduction with H_2 [90, 91].

Untreated, aerobic enzyme showed several IR bands in the 2,120–1,880 cm^{-1} region (Fig. 6, trace A). In the ν(CO) region, a strong band at 1,962 cm^{-1} with a shoulder at 1,955 cm^{-1} and a weak band at 1,929 cm^{-1} were present. In the ν(CN) region, three bands at 2,104, 2,086 and 2,055 cm^{-1} were observed with a shoulder at 2,078 cm^{-1}. The ν(CO) region changed after keeping the enzyme in the IR cell at 4 °C for 3 days (Fig. 6, trace B): the 1,955-cm^{-1} band considerably decreased, the 1,929-cm^{-1} band disappeared and a weak band at 1,980 cm^{-1} showed up. The ν(CN) region did not change. Enzyme mixed with 2 mM 2,6-dichlorophenol-indophenol (DCIP), to optimally oxidize the HoxYH enzyme, had a similar effect, although the 1,929-cm^{-1} band was not affected (Fig. 6, trace C). The slight decrease in amplitude of the bands was caused by dilution. After an additional period of 19 h at room temperature, the spectrum hardly changed (Fig. 6, trace D).

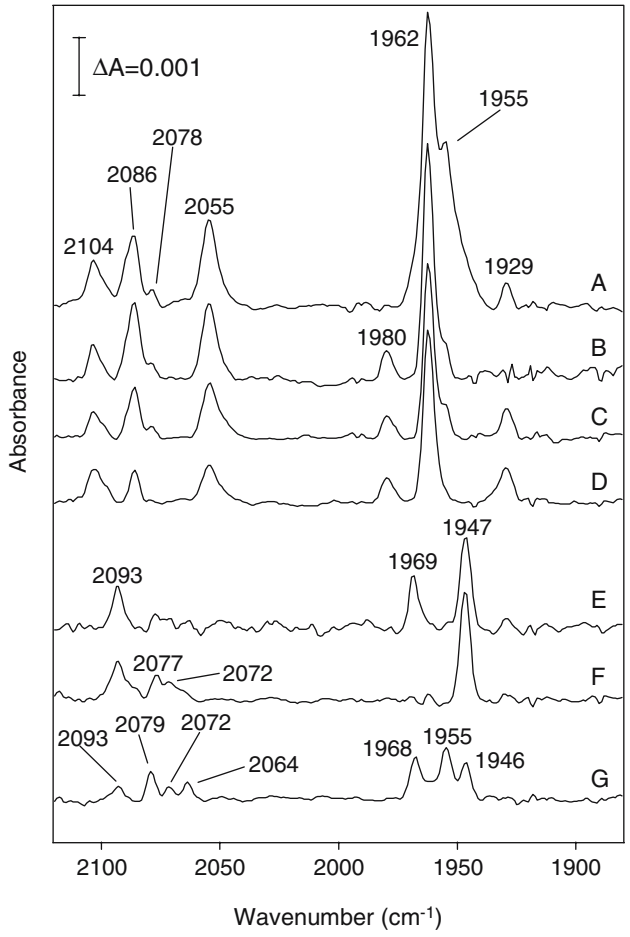

Fig. 6 IR spectra at room temperature in the 2,120–1,880-cm^{-1} spectral region of the HoxYH enzyme. *A* Enzyme as isolated. *B* After 3 days in the IR cell at 4 °C. *C* Enzyme treated with 2 mM 2,6-dichlorophenol-indophenol for 1 h at room temperature. *D* Same sample after an additional 19 h at room temperature. *E* Enzyme reduced with 20 mM dithionite under an Ar atmosphere during 2 h at room temperature. *F* Same sample after an additional 1.5 h at room temperature. *G* Enzyme reduced with 20 mM dithionite under 1 bar CO during 5 h at room temperature

Reduction of the HoxYH enzyme with 20 mM dithionite under an Ar atmosphere during 2 h at room temperature resulted in replacement of the three bands in the ν(CO) region by two bands at 1,969 and 1,947 cm^{-1} (Fig. 6, trace E). In the ν(CN) region, the prominent band at 2,055 cm^{-1} disappeared and only one band at 2,093 cm^{-1} was observed. After an additional period of 1.5 h at room temperature, the band at 1,969 cm^{-1} disappeared (Fig. 6, trace F). Because of the poor signal-to-noise ratio in the cyanide region of trace E, it cannot be excluded that the two weak bands around 2,077 and 2,072 cm^{-1} in trace F were already present in trace E of Fig. 6.

Reduction of enzyme with 20 mM dithionite under a CO atmosphere for 5 h at room temperature caused a quite different spectrum (Fig. 6, trace G). Three bands were observed in the ν(CO) region (at 1,968, 1,955 and 1,946 cm^{-1}), whereas four weaker bands were noticed in the ν(CN) region (at 2,093, 2,079, 2,072 and 2,064 cm^{-1}).

When the areas of the ν(CO) peaks around 1,950 cm^{-1} in Fig. 6 were determined (via curve fitting) and compared with the area of the ν(CO) peak in an IR spectrum of the *A. vinosum* MBH of known concentration, the calculated HoxYH concentrations were approximately 0.5, 0.2 and 0.1 mM for the samples used for traces A, B and C, and E–G, respectively. The assumption was made that the intrinsic COs in both enzymes give rise to the same IR intensity. These concentrations are of importance for the possible explanation of the low EPR signal intensities found for the Ni and Fe–S signals (see "Discussion").

Discussion

We start with a few initial remarks about the purification procedure. The Amsterdam laboratory had earlier inspected the second hydrogenase activity from *A. vinosum*. Upon partial purification of this soluble activity, a preparation was obtained that showed both a H_2-production activity and an NADH–$K_3Fe(CN)_6$ activity. Addition of NADH induced a rhombic EPR signal from a [2Fe–2S] cluster plus a radical signal (J. W. van der Zwaan, as referred to in [57]). No EPR signals of nickel were seen. We have spent a considerable amount of time trying to purify fractions containing both activities. We noticed that on the first DEAE column, the NADH–$K_3Fe(CN)_6$ and hydro-

genase activities stayed together only when the acetone-powder extract was not too dilute. However, in that case the binding of the hydrogenase activity to the column was weak, prohibiting the preparation of sufficient quantities of enzyme for spectroscopic studies. For a good binding, a rather large dilution was required. In that case both activities did not move together. Addition of 1 mM $NiCl_2$ to the extract had no effect. We conclude that the HoxYH and HoxEFU modules of the *A. vinosum* enzyme are only loosely bound. This is reminiscent of the HoxFUYH enzyme from *Rhodococcus opacus* (formerly *Nocardia opaca*), which easily dissociates into HoxFU and HoxYH dimers [92, 93]. The related $HoxFUYHI_2$ enzyme from *R. eutropha* readily loses the HoxI subunits, but does not further dissociate as tested under a variety of redox and/or dilution conditions [78].

The HoxFU module in the *R. eutropha* and *R. opacus* enzymes catalyses a NADH–$K_3Fe(CN)_6$ activity. Assuming that this activity in the *A. vinosum* cell-free extract is, at least in part, due to the HoxEFU module, then it is curious to note that we could not measure any H_2–NAD^+ activity. It has been reported that such an activity was only measurable when a soluble electron carrier (e.g. ferredoxin from *C. pasteurianum* or *A. vinosum*, or BV) was added [38]; hence, the apparent dissociation of the *A. vinosum* HoxEFUYH complex may already occur upon opening of the cells. The purified reversible hydrogenase of *Anabaena variabilis* ATCC 29413, which is now known to be a HoxEFUYH [NiFe] hydrogenase, contains FMN and the reduced enzyme exhibits EPR signals of at least one type of [2Fe–2S] cluster, one type of [4Fe–4S] cluster, but no signals from nickel [94]. Apparently, the HoxEFUYH enzymes from *Cyanobacteria* are much stabler, because two more enzymes have been successfully purified from *Synechocystis* and *Synechococcus* [46].

Possible structural composition of the *A. vinosum* HoxEFUYH complex

We have demonstrated that the *A. vinosum* HoxEFUYH complex has the binding sites for three [2Fe–2S] clusters and five [4Fe–4S] clusters. The amino acid sequences of the subunits have their counterparts in subunits of complex I, and that of HoxU also in the N-terminal part of the *C. pasteurianum* [FeFe] hydrogenase I.

The crystal structure (at 4-Å resolution) of the hydrophilic domain of complex I from *T. thermophilus*, containing all Fe–S clusters of the intact complex I, was published last year [50]. The 3.3-Å structure was published recently [51]. In Fig. 7, we compare the arrangement of the Fe–S clusters in this domain (panel I) with that of the *C. pasteurianum* [FeFe] hydrogenase (panel II). It can be seen that within the red dashed ovals the structural arrangement of the [2Fe–2S] and the two [4Fe–4S] clusters in both enzymes is highly similar, as was described (but not shown) by Sazanov and Hinchliffe [51]. These clusters are bound to the N-terminal regions of the 75-kDa subunit (called Nqo3 for *T. thermophilus*) of complex I and that of the [FeFe] hydrogenase I (Table 2). Even although the 75-kDa subunit of complex I does not have the cysteine motif for binding an analogue of the medial cluster in the [FeFe] hydrogenase, the number of amino acids between the first three cysteine residues binding the distal-cluster analogue and the conserved CP couple, where the cysteine residue acts as the fourth ligand to this cluster, is the same [74] and this resulted in the conservation of the structure of this polypeptide piece [51]. We predict that the structure of the HoxU subunit and its arrangement of the Fe–S clusters (Fig. 8) is highly similar to that of the N-terminal part of the *C. pasteurianum* [FeFe] hydrogenase (green oval in Fig. 7, panel II). Although Fig. 7 may suggest that the [4Fe–4S] cluster labeled as 'Extra' in the complex I structure (extra, because this cluster is not present in bovine complex I and many others) could be related to the $[4Fe–4S]_H$ subcluster being part of the H cluster in [FeFe] hydrogenases, this can be ruled out by the sequence comparisons, because the cysteine motifs binding these clusters are completely different.

In complex I, a second [2Fe–2S] cluster is present in the 24-kDa subunit (encircled green; upper left in Fig. 7, panel I). This subunit is highly similar to the HoxE subunit (Table 2). The 51-kDa (Nqo1) subunit contains a [4Fe–4S] cluster plus FMN [51]. This is in agreement with early studies on an enzyme, called the low molecular weight NADH dehydrogenase, prepared from bovine complex I. This consisted of the 51-, 24- and 9-kDa subunits [95] and contained two NADH-reducible Fe–S clusters with the typical EPR characteristics of a [4Fe–4S] and a [2Fe–2S] cluster [70]. The [2Fe–2S] cluster was shown to reside in the 24 + 9-kDa subcomplex. The HoxF subunits have the same binding domains for FMN/NAD(H) and a [4Fe–4S] cluster as the 51-kDa (Nqo1) subunit (Table 2); hence, we propose that the HoxEFU module of the *A. vinosum* HoxEFUYH complex is structurally similar to the centre plus the top-left parts of complex I in Fig. 7, panel I. This is depicted in Fig. 8. We note that the *A. vinosum* HoxF has an extra binding site for a [2Fe–2S] cluster (absent in complex I and in HoxF from *R. eutropha*). The spatial position of this cluster cannot be predicted because it is bound by an N-terminal

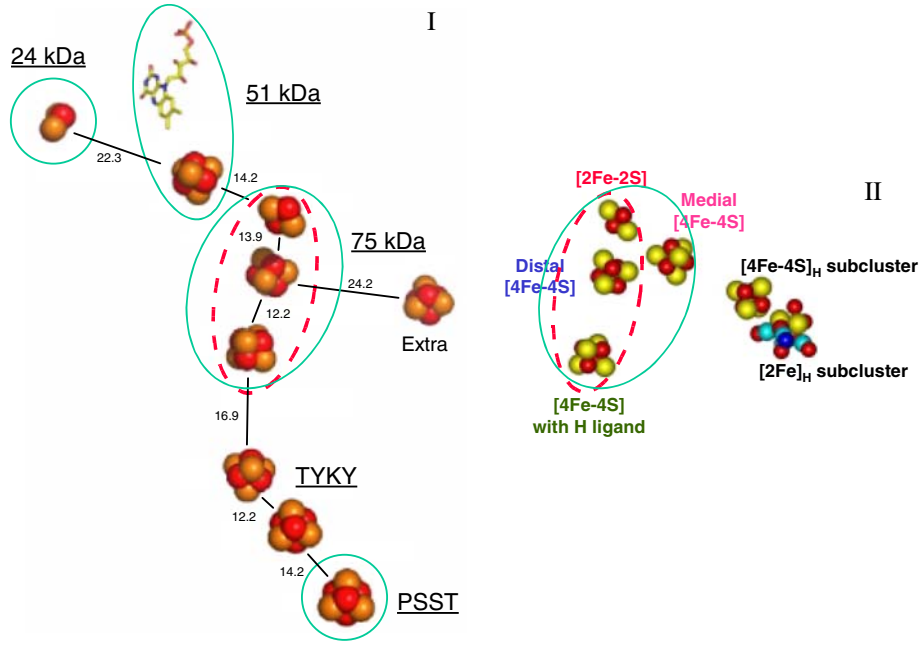

Fig. 7 Comparison of the structures of complex I from *Thermus thermophilus* [51] and the [FeFe] hydrogenase I from *Clostridium pasteurianum* [2] as a basis for the prediction of the relative positions of the prosthetic groups of the *A. vinosum* HoxEFUYH complex shown in Fig. 8. *Panel I*: 2D image of the prosthetic groups in the hydrophilic domain of *T. thermophilus* complex I (adapted from [51]). The subunit names are those from the bovine enzyme. The *T. thermophilus* names are as follows: 24 kDa, Nqo2; 51 kDa, Nqo1; 75 kDa, Nqo3; TYKY, Nqo9; PSST, Nqo6. The cubane cluster denoted as *Extra* is not present in bovine complex I. The distances (in Å) between the centres of the Fe–S clusters are taken from [51]. *Panel II*: Prosthetic groups in the *C. pasteurianum* hydrogenase I [2]. Coordinates were taken from the structure file (PDB entry 1feh). The 3D structure is represented such that the iron and sulfur atoms of three of the Fe–S clusters in the N-terminal domain optimally superimpose upon those of the 75-kDa subunit in the 2D image of complex I (*red dashed ovals*). The *green circles*/*ovals* indicate flavin mononucleotide (*FMN*) and/or Fe–S clusters, the binding sites of which are also present in the *A. vinosum* HoxEFUYH complex

extension in HoxF which is absent in the 51-kDa (Nqo1) subunits. One possibility is that it forms an electronic bridge between the [2Fe–2S] cluster in HoxE (24 kDa) and the [4Fe–4S] cluster in HoxF (51 kDa). In complex I, the distance between the two relevant clusters is 22.3 Å and this is considered inadequate for fast electron transfer [50, 51]. An intermediate [2Fe–2S] cluster would repair the electronic contact. The spatial positions of the Fe–S clusters in the HoxU subunit (Fig. 8) can be predicted by comparison with the structures of complex I and the *C. pasteurianum* [FeFe] hydrogenase I (Fig. 7).

The remaining HoxYH subunits form the hydrogenase module of the soluble [NiFe] hydrogenase. Structurally this part can be compared with standard [NiFe] hydrogenases. A first possibility for direct attachment of the HoxYH module to the HoxEFU module is via the medial cluster in the structural analogue of the [FeFe] hydrogenase in HoxU (possibility A in Fig. 8). In that case the [4Fe–4S] cluster and the Ni–Fe site in the HoxYH subunits would 'replace' the H cluster as an H_2-reactive centre (cf. Fig. 7, panel II). A second possible point for a direct attachment is via the [4Fe–4S] cluster with the histidine ligand in HoxU (not shown). In both cases the complex would be expected to show H_2–NAD^+ activity.

In complex I, the link between the HoxYH homologues (the PSST and 49-kDa subunits, respectively) and the HoxU homologue (the 75-kDa subunit) appears to be formed by the TYKY (Nqo9) subunit with its two [4Fe–4S] clusters [51] (Fig. 7, panel I); hence, a third tentative possibility is to assume that the intact HoxEFUYH complex in the cell has an attached 2[4Fe–4S] ferredoxin, e.g. the *A. vinosum* ferredoxin, shunting between the HoxYH module and the HoxEFU module in an arrangement similar to the homologous subunits in complex I (possibility B in Fig. 8; the two hypothetical [4Fe–4S] clusters are not shown). In this connection, it is worthwhile mentioning the possibility that in the energy-converting [NiFe] hydrogenase (Ech) from *Methanosarcina barkeri* [96–99] the hydrogenase module [EchC and EchE subunits, homologues of the PSST (HoxY) and 49 kDa (HoxH) subunits, respectively] may be attached to the EchF subunit, a homologue of the TYKY (Nqo9) subunit, in a way similar to that in complex I.

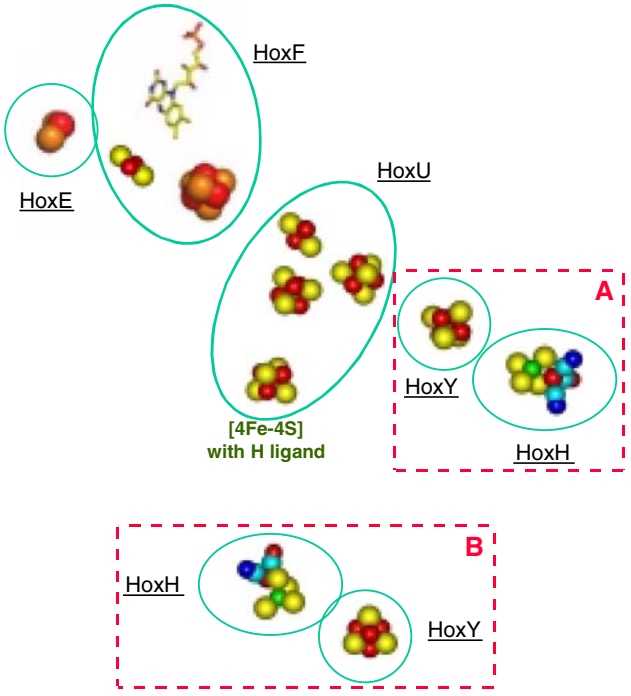

Fig. 8 Tentative spatial arrangement of the predicted prosthetic groups (FMN and Fe–S clusters) in the HoxEFUYH [NiFe] hydrogenase from *A. vinosum*. The positions of the 2Fe cluster in HoxE, and of the FMN and the 4Fe cluster in HoxF, are taken from the 2D image of complex I in Fig. 7, panel I. The position of the extra 2Fe cluster in HoxF is arbitrary. The unit with the four Fe–S clusters in HoxU is taken from the 2D image of the [FeFe] hydrogenase structure in Fig. 7, panel II. The structures of the 4Fe cluster in HoxY and the Ni–Fe centre in HoxH, as well as their relative positions, are taken from the structure of the *Desulfovibrio gigas* [NiFe] hydrogenase [10] (PDB entry 2frv). Two possible positions of the HoxYH module are shown (*red dashed rectangles*). In position *A* the iron and sulfur atoms of the 4Fe cluster were superimposed on those of the $[4Fe–4S]_H$ subcluster in the structure of [FeFe] hydrogenase (cf. structure in Fig. 7, panel II) such that the Ni–Fe centre pointed in the direction of the $[2Fe]_H$ subcluster. In position *B* the iron and sulfur atoms were superimposed on those of the cubane cluster in the PSST subunit of the complex I structure (Fig. 7, panel I) such that the Ni–Fe centre pointed to the direction of the position of the 49-kDa subunit [51] (homologue of HoxH) of complex I (not indicated in Fig. 7, panel I)

Summarizing, we propose that the *A. vinosum* HoxEFUYH [NiFe] hydrogenase is structurally related to most of the hydrophilic domain of complex I and shares six of its Fe–S clusters. Reduction of all Fe–S clusters in bovine complex I by NADH is a very fast reaction. Pre-steady-state kinetics experiments show that reduction is completed within the dead time of the freeze–quench machine (5 ms) even at 4 °C [81, 100]. The recent structure of the hydrophilic domain of complex I from *T. thermophilus* [50, 51] suggests that this submillisecond electron transfer covers a distance of over 140 Å. At present it is unclear whether the HoxEFUYH types of [NiFe] hydrogenases also have such a property and why they would need this. Upon opening of the *A. vinosum* cells, resulting in a dilution of the cell contents, there is no measurable H_2–NAD^+ activity (unless electron carriers are added [36, 38], e.g. the *A. vinosum* ferredoxin [37], a 2[4Fe–4S] protein [101]). This prevents further study of the electron-transfer properties.

EPR properties of the HoxYH enzyme

The protein concentrations used for the EPR experiments (40–60 mg ml^{-1}) predict enzyme concentrations of 550–800 μM, assuming that the preparations were completely pure. The spin concentration of the EPR signals assigned to the Ni–Fe site and the proximal [4Fe–4S] cluster amounted, however, only to 4–6 μM, i.e. two orders of magnitude less. We note that the HoxYH enzyme from the large-scale purification had the same (even somewhat higher) specific activity as the nearly pure enzyme from the small-scale purification. This, and the fact that the IR spectra indicated that the concentration of the Ni–Fe site was at least one order of magnitude greater than the EPR-derived concentrations, led us to conclude that the majority of the molecules in the oxidized enzyme do not have an EPR-detectable Ni centre. This also indicates that the midpoint potential of the proximal cluster is presumably considerably lower than that of the normal hydrogen electrode. The latter property would be in agreement with a H_2-production function of the enzyme. However, these initial results remain to be verified.

The EPR spectra indicate that the enzyme preparation was not pure. Very weak signals around $g = 6$ point to the presence of traces of high-spin haem proteins. The amount of these signals varied with the preparation. The most intriguing signal in all three preparations was the strong $g = 4$ signal. In the preparation used for Fig. 5 it amounted to about 320 μM. The signal is indistinguishable from that of the Fe superoxide dismutases from *M. bryanti* [102] and several other microorganisms [103–105]. Assuming that such a protein, with a molecular mass of 22 kDa, is the major contaminant, then this would amount to 7 mg ml^{-1} in the EPR tube, i.e. 12–18% of the protein. This would, however, not invalidate the conclusions made before about the properties of the Ni–Fe site and the proximal cluster. Although it cannot be excluded, it is highly surprising that an Fe superoxide dismutase would copurify with the HoxYH enzyme. Hence, another tentative possibility to explain the strong $g = 4$ signal is to assume that the low-spin Fe^{2+} in the Ni–Fe

site has turned into a high-spin Fe^{3+} by the loss of one or more of its diatomic ligands.

IR properties of the HoxYH enzyme

We do not understand the origin of the band at 1,955 cm^{-1} (in untreated enzyme; Fig. 6, trace A) that largely disappeared in time (Fig. 6, trace B) or upon addition of excess DCIP. Also the origin of the rather strong band at 2,055 cm^{-1} in the oxidized enzyme is unclear. In standard [NiFe] hydrogenases, a band close to this position is seen in three cases: (1) a ν(CN) band in H_2-reduced enzyme [106, 107]; (2) a ν(CN) band in the so-called Ni_a–L* state [106, 107]; (3) a ν(CO) band of extrinsic CO bound to nickel [11, 12]. Because this band persisted in HoxYH enzyme after treatment with DCIP, it is unlikely to be caused by a ν(CN) band from reduced enzyme. This is in agreement with the fact that the band disappeared upon reduction (Fig. 6). The Ni_a–L* state can also be ruled out as a source, because that state is only stable at cryogenic temperatures. Also the third possibility is unlikely, because no 2,055-cm^{-1} band was observed in CO-treated enzyme (see below). It cannot be ruled out that this band is due to the species that shows the $g = 4$ EPR signal.

Reduction with dithionite resulted in replacement of the ν(CO) band at 1,962 cm^{-1} of the oxidized enzyme by bands at 1,969 and 1,947 cm^{-1}. The 1,969-cm^{-1} band is presumably an intermediate redox state of the Ni–Fe centre, possibly the Ni_a–S state, because only the 1,947-cm^{-1} band remained present at longer times. The latter band is assigned to the fully reduced state of the Ni–Fe centre (Ni_a–SR state).

The CO inhibition of the HoxYH enzyme (Fig. 4) is in agreement with the general CO sensitivity of [NiFe] hydrogenases. In standard [NiFe] hydrogenases, CO binds to nickel [86] and so this is also expected for the HoxYH enzyme. We tentatively assign the band at 2,064 cm^{-1} in Fig. 6, trace G, from CO-treated enzyme, to extrinsic CO bound to nickel.

Acknowledgements M.L. was supported by grants from the National Natural Science Foundation of China (30470395) and the National 863 Project of China (2002AA515030). S.P.J.A. thanks the Netherlands Organization for Scientific Research (NWO), Division of Chemical Sciences, for support. We thank A.O.M. Muijsers for the N-terminal sequencing work.

References

1. Adams MW (1990) Biochim Biophys Acta 1020:115–145
2. Peters JW, Lanzilotta WN, Lemon BJ, Seefeldt LC (1998) Science 282:1853–1858
3. Nicolet Y, Piras C, Legrand P, Hatchikian EC, Fontecilla-Camps JC (1999) Struct Fold Des 7:13–23
4. Van der Spek TM, Arendsen AF, Happe RP, Yun S, Bagley KA, Stufkens DJ, Hagen WR, Albracht SPJ (1996) Eur J Biochem 237:629–634
5. Pierik AJ, Hulstein M, Hagen WR, Albracht SPJ (1998) Eur J Biochem 258:572–578
6. Albracht SPJ, Roseboom W, Hatchikian EC (2006) J Biol Inorg Chem 11:88–101
7. Roseboom W, De Lacey AL, Fernandez VM, Hatchikian EC, Albracht SPJ (2006) J Biol Inorg Chem 11:102–118
8. Albracht SPJ (1994) Biochim Biophys Acta 1188:167–204
9. Volbeda A, Charon MH, Piras C, Hatchikian EC, Frey M, Fontecilla-Camps JC (1995) Nature 373:580–587
10. Volbeda A, Garcia E, Piras C, De Lacey AL, Fernandez VM, Hatchikian EC, Frey M, Fontecilla-Camps JC (1996) J Am Chem Soc 118:12989–12996
11. Bagley KA, Van Garderen CJ, Chen M, Duin EC, Albracht SPJ, Woodruff WH (1994) Biochemistry 33:9229–9236
12. Bagley KA, Duin EC, Roseboom W, Albracht SPJ, Woodruff WH (1995) Biochemistry 34:5527–5535
13. Happe RP, Roseboom W, Pierik AJ, Albracht SPJ, Bagley KA (1997) Nature 385:126
14. Pierik AJ, Roseboom W, Happe RP, Bagley KA, Albracht SPJ (1999) J Biol Chem 274:3331–3337
15. Lyon EJ, Shima S, Böcher R, Thauer RK, Grevels FW, Bill E, Roseboom W, Albracht SPJ (2004) J Am Chem Soc 126:14239–14248
16. Shima S, Lyon EJ, Thauer RK, Mienert B, Bill E (2005) J Am Chem Soc 127:10430–10435
17. Cammack R, Frey M, Robson R (2001) Hydrogen as a fuel. Learning from nature. Taylor & Francis, London
18. Vignais PM, Colbeau A (2004) Curr Issues Mol Biol 6:159–188
19. De Lacey AL, Hatchikian EC, Volbeda A, Frey M, Fontecilla-Camps JC, Fernandez VM (1997) J Am Chem Soc 119:7181–7189
20. Rousset M, Montet Y, Guigliarelli B, Forget N, Asso M, Bertrand P, Fontecilla-Camps JC, Hatchikian EC (1998) Proc Natl Acad Sci USA 95:11625–11630
21. Garcin E, Vernède X, Hatchikian EC, Volbeda A, Frey M, Fontecilla-Camps JC (1999) Struct Fold Des 7:557–566
22. Matias PM, Soares CM, Saraiva LM, Coelho R, Morais J, Le Gall J, Carrondo MA (2001) J Biol Inorg Chem 6:63–81
23. Fernandez VM, Hatchikian EC, Cammack R (1985) Biochim Biophys Acta 832:69–79
24. Fernandez VM, Rao KK, Fernandez MA, Cammack R (1986) Biochimie 68:43–48
25. Kurkin S, George SJ, Thorneley RNF, Albracht SPJ (2004) Biochemistry 43:6820–6831
26. Lamle SE, Albracht SPJ, Armstrong FA (2004) J Am Chem Soc 126:14899–14909
27. Lamle SE, Albracht SPJ, Armstrong FA (2005) J Am Chem Soc 127:6595–6604
28. Bleijlevens B, Faber BW, Albracht SPJ (2001) J Biol Inorg Chem 6:763–769
29. Volbeda A, Martin L, Cavazza C, Matho M, Faber BW, Roseboom W, Albracht SPJ, Garcin E, Rousset M, Fontecilla-Camps JC (2005) J Biol Inorg Chem 10:239–249
30. Ogata H, Hirota S, Nakahara A, Komori H, Shibata N, Kato T, Kano K, Higuchi Y (2005) Structure 13:1635–1642
31. Ackrell BA, Asato RN, Mower HF (1966) J Bacteriol 92:828–838
32. Rossmann R, Sauter M, Lottspeich F, Böck A (1994) Eur J Biochem 220:377–384
33. Andrews SC, Berks BC, McClay J, Ambler A, Quail MA, Golby P, Guest JR (1997) Microbiology 143:3633–3647

34. Robson R (2001) In: Cammack R, Frey M, Robson R (eds) Hydrogen as a fuel. Learning from nature. Taylor & Francis, London, pp 9–32
35. Buchanan BB, Bachofen R, Arnon DI (1964) Biochemistry 52:839–847
36. Weaver P, Tinker K, Valentine RC (1965) Biochem Biophys Res Commun 21:195–201
37. Buchanan BB, Bachofen R (1968) Biochim Biophys Acta 162:607–610
38. Feigenblum E, Krasna AI (1970) Biochim Biophys Acta 198:157–164
39. Llama MJ, Serra JL, Rao KK, Hall DO (1981) Eur J Biochem 114:89–96
40. George SJ, Kurkin S, Thorneley RNF, Albracht SPJ (2004) Biochemistry 43:6808–6819
41. Surerus KK, Chen M, van der Zwaan JW, Rusnak FM, Kolk M, Duin EC, Albracht SPJ, Münck E (1994) Biochemistry 33:4980–4993
42. Gu ZJ, Dong J, Allan CB, Choudhury SB, Franco R, Moura JJG, LeGall J, Przybyla AE, Roseboom W, Albracht SPJ, Axley MJ, Scott RA, Maroney MJ (1996) J Am Chem Soc 118:11155–11165
43. Davidson G, Choudhury SB, Gu Z, Bose K, Roseboom W, Albracht SPJ, Maroney MJ (2000) Biochemistry 39:7468–7479
44. Schmitz O, Boison G, Hilscher R, Hundeshagen B, Zimmer W, Lottspeich F, Bothe H (1995) Eur J Biochem 233:266–276
45. Boison G, Bothe H, Hansel A, Lindblad P (1999) FEMS Microbiol Lett 174:159–165
46. Schmitz O, Boison G, Salzmann H, Bothe H, Schutz K, Wang SH, Happe T (2002) Biochim Biophys Acta 1554:66–74
47. Tamagnini P, Axelsson R, Lindberg P, Oxelfelt F, Wunschiers R, Lindblad P (2002) Microbiol Mol Biol Rev 66:1–20
48. Schutz K, Happe T, Troshina O, Lindblad P, Leitao E, Oliveira P, Tamagnini P (2004) Planta 218:350–359
49. Rákhely G, Kovács AT, Maróti G, Fodor BD, Csanádi G, Latinovics D, Kovács KL (2004) Appl Environ Microbiol 70:722–728
50. Hinchliffe P, Sazanov LA (2005) Science 309:771–774
51. Sazanov LA, Hinchliffe P (2006) Science 311:1430–1436
52. Hinchliffe P, Carroll J, Sazanov LA (2006) Biochemistry 45:4413–4420
53. Van Heerikhuizen H, Albracht SPJ, Slater EC, van Rheenen PS (1981) Biochim Biophys Acta 657:26–39
54. Hendley DD (1955) J Bacteriol 70:625–634
55. Albracht SPJ, Kalkman ML, Slater EC (1983) Biochim Biophys Acta 1983:309–316
56. Kovács KL, Tigyi G, Alfonz H (1985) Prep Biochem 15:321–334
57. Coremans JMCC, van der Zwaan JW, Albracht SPJ (1992) Biochim Biophys Acta 1119:157–168
58. Lowry OH, Rosebrough NJ, Farr AL, Randall RJ (1951) J Biol Chem 193:265–275
59. Coremans JMCC, Van der Zwaan JW, Albracht SPJ (1989) Biochim Biophys Acta 997:256–267
60. Studier FW (1973) J Mol Biol 79:237–248
61. Laemmli UK (1970) Nature 227:680–685
62. Jacobson FS, Daniels L, Fox JA, Walsh CT, Orme-Johnson WH (1982) J Biol Chem 257:3385–3388
63. Adams MW, Hall DO (1979) Arch Biochem Biophys 195:288–299
64. Matsudaira P (1987) J Biol Chem 262:10035–10038
65. Sambrook J, Maniatis T, Fritsch EF (1989) Molecular cloning: a laboratory manual. Cold Spring Harbor Laboratory Press, Cold Spring Harbor
66. Happe RP, Roseboom W, Albracht SPJ (1999) Eur J Biochem 259:602–608
67. Altschul SF, Madden TL, Schaffer AA, Zhang J, Zhang Z, Miller W, Lipman DJ (1997) Nucleic Acids Res 25:3389–3402
68. Thompson JD, Gibson TJ, Plewniak F, Jeanmougin F, Higgins DG (1997) Nucleic Acids Res 25:4876–4882
69. Ohnishi T, Blum H, Galante YM, Hatefi Y (1981) J Biol Chem 256:9216–9220
70. Ragan CI, Galante YM, Hatefi Y, Ohnishi T (1982) Biochemistry 21:590–594
71. Ohnishi T, Ragan CI, Hatefi Y (1985) J Biol Chem 260:2782–2788
72. Pilkington SJ, Skehel JM, Gennis RB, Walker JE (1991) Biochemistry 30:2166–2175
73. Bottoms CA, Smith PE, Tanner JJ (2002) Protein Sci 11:2125–2137
74. Albracht SPJ, De Jong AMP (1997) Biochim Biophys Acta 1318:92–106
75. Arizmendi JM, Runswick MJ, Skehel JM, Walker JE (1992) FEBS Lett 301:237–242
76. Fearnley IM, Walker JE (1992) Biochim Biophys Acta 1140:105–134
77. Albracht SPJ, Hedderich R (2000) FEBS Lett 485:1–6
78. Van der Linden E, Faber BW, Bleijlevens B, Burgdorf T, Bernhard M, Friedrich B, Albracht SPJ (2004) Eur J Biochem 271:801–808
79. Van der Linden E, Burgdorf T, De Lacey AL, Buhrke T, Scholte M, Fernandez VM, Friedrich B, Albracht SPJ (2006) J Biol Inorg Chem 11:247–260
80. Albracht SPJ, Van der Linden E, Faber BW (2003) Biochim Biophys Acta 1557:41–49
81. Van Belzen R, Albracht SPJ (1989) Biochim Biophys Acta 974:311–320
82. Burgdorf T, Van der Linden E, Bernhard M, Yin QY, Back JW, Hartog AF, Muijsers AO, de Koster CG, Albracht SPJ, Friedrich B (2005) J Bacteriol 187:3122–3132
83. Montet Y, Amara P, Volbeda A, Vernede X, Hatchikian EC, Field MJ, Frey M, Fontecilla-Camps JC (1997) Nat Struct Biol 4:523–526
84. Higuchi Y, Yagi T, Yasuoka N (1997) Structure 5:1671–1680
85. Higuchi Y, Ogata H, Miki K, Yasuoka N, Yagi T (1999) Struct Fold Des 7:549–556
86. Ogata H, Mizoguchi Y, Mizuno N, Miki K, Adachi S, Yasuoka N, Yagi T, Yamauchi O, Hirota S, Higuchi Y (2002) J Am Chem Soc 124:11628–11635
87. Volbeda A, Montet Y, Vernède X, Hatchikian EC, Fontecilla-Camps JC (2002) Int J Hydrogen Energy 27:1449–1461
88. Strekas T, Antanaitis BC, Krasna AI (1980) Biochim Biophys Acta 616:1–9
89. Vänngård T (1972) In: Swartz HM, Bolton JR, Borg DC (eds) Biological applications of electron spin resonance. Wiley, New York, pp 411–447
90. Coremans JMCC, van Garderen CJ, Albracht SPJ (1992) Biochim Biophys Acta 1119:148–156
91. Duin EC (1996) PhD thesis, University of Amsterdam
92. Schneider K, Cammack R, Schlegel HG (1984) Eur J Biochem 142:75–84
93. Schneider K, Schlegel HG, Jochim K (1984) Eur J Biochem 138:533–541
94. Serebryakova LT, Medina M, Zorin NA, Gogotov IN, Cammack R (1996) FEBS Lett 383:79–82

95. Galante YM, Hatefi Y (1979) Arch Biochem Biophys 192:559–568
96. Kunkel A, Vorholt JA, Thauer RK, Hedderich R (1998) Eur J Biochem 252:467–476
97. Meuer J, Kuettner HC, Zhang JK, Hedderich R, Metcalf WW (2002) Proc Natl Acad Sci USA 99:5632–5637
98. Kurkin S, Meuer J, Koch J, Hedderich R, Albracht SPJ (2002) Eur J Biochem 269:6101–6111
99. Forzi L, Koch J, Guss AM, Radosevich CG, Metcalf WW, Hedderich R (2005) FEBS J 272:4741–4753
100. Orme-Johnson NR, Hansen RE, Beinert H (1974) J Biol Chem 249:1922–1927
101. Kyritsis P, Hatzfeld OM, Link TA, Moulis JM (1998) J Biol Chem 273:15404–15411
102. Kirby TW, Lancaster JR Jr, Fridovich I (1981) Arch Biochem Biophys 210:140–148
103. Renault JP, Verchère-Béaur C, Morgenstern-Badarau I, Yamakura F, Gerloch M (2000) Inorg Chem 39:2666–2675
104. Gratepanche S, Ménage S, Touati D, Wintjens R, Delplace P, Fontecave M, Masset A, Camus D, Dive D (2002) Mol Biochem Parasitol 120:237–246
105. Kerfeld CA, Yoshida S, Tran KT, Yeates TO, Cascio D, Bottin H, Berthomieu C, Sugiura M, Boussac A (2003) J Biol Inorg Chem 8:707–714
106. Albracht SPJ (2001) In: Cammack R, Frey M, Robson R (eds) Hydrogen as a fuel. Learning from nature. Taylor & Francis, London, pp 110–158
107. Bleijlevens B, van Broekhuizen FA, De Lacey AL, Roseboom W, Fernandez VM, Albracht SPJ (2004) J Biol Inorg Chem 9:743–752